


Cite this: *Sustainable Food Technol.*,
2025, 3, 677

Chitin nanofibers derived from deep eutectic solvent extraction and ammonium persulfate oxidation as a seed nanopriming agent for microgreen growth enhancement

Honglin Zhu, Sunni Chen, Jingyi Xue, Ruiqi Wang, Xinhao Wang, Zhenlei Xiao* and Yangchao Luo *

Chitin nanofibers (ChNFs) were successfully prepared from lobster shells using deep eutectic solvents (DESs) and ammonium persulfate oxidation (APS), offering a sustainable approach for marine waste utilization. DES-treated chitin (DES-Chitin) with a yield of 26.22% and 94.78% purity retained a high degree of acetylation (96%), while APS oxidation improved crystallinity, introduced carboxyl content, and enhanced dispersibility. The resulting ChNFs obtained after 5 hours of APS oxidation (5h-ChNFs) exhibited superior transparency, dispersion stability, and morphological refinement, with thermal stability comparable to DES-Chitin. In germination studies, 5h-ChNFs significantly improved physiological characteristics, nitrogen assimilation, and chlorophyll synthesis in broccoli and radish microgreens. Optimal concentrations of 20 $\mu\text{g mL}^{-1}$ for broccoli and 75 $\mu\text{g mL}^{-1}$ for radish enhanced protein, polyphenol, and flavonoid contents, alongside elevated DPPH and ABTS radical scavenging capacities. These findings demonstrated the potential of ChNFs as a bioactive seed nanopriming agent, bridging nanomaterial science and agricultural biotechnology to increase microgreen production sustainably.

Received 28th January 2025
Accepted 11th March 2025

DOI: 10.1039/d5fb00026b

rsc.li/susfoodtech

Sustainability spotlight

The extraction and preparation of chitin nanofibers (ChNFs) from lobster shells using eco-friendly deep eutectic solvents and ammonium persulfate offers a green alternative to traditional methods. This innovative process yields high-purity chitin without harsh chemicals, aligning with circular economy principles by converting seafood waste into valuable agricultural inputs. Compared to raw chitin, 5h-ChNFs demonstrate enhanced crystallinity, dispersibility, and functional properties, making them highly effective in boosting the growth of broccoli and radish microgreens *via* seed priming. Their nano-scale structure improves water dispersibility and nutrient uptake during seed germination and seedling development, while their biodegradable nature minimizes environmental impact. By reducing reliance on synthetic inputs, ChNFs promote sustainable technology and efficient resource utilization of food waste.

1 Introduction

Chitin, a natural polysaccharide abundantly found in crustacean shells, insects, and microorganisms, is a versatile biopolymer with significant applications in food and agriculture.¹ However, traditional methods of chitin extraction from sources such as lobster shells often require harsh chemical treatments, which pose environmental risks and hinder their alignment with sustainable industrial practices. In recent years, deep eutectic solvents (DESs) have emerged as a promising green alternative due to their non-toxic, biodegradable, and recyclable nature.² DESs have proven effective in simplifying the demineralization and deproteination processes necessary for

high-purity chitin extraction, offering a more environmentally friendly solution.³

Despite its versatility, the application of chitin in food and agriculture is often limited by its poor solubility in common solvents and low biodegradability. To address these challenges, nanostructured chitin, particularly in the form of chitin nanofibers (ChNFs), has gained considerable attention. ChNFs exhibited enhanced properties, including high dispersibility in water, a high specific surface area, low density, and excellent formability.⁴ Various methods, such as ultrasonication,⁵ grinding,⁶ microfluidization,⁷ TEMPO oxidation,⁸ ionic liquid hydrolysis,⁹ and ammonium persulfate (APS) oxidation,¹⁰ are employed to produce ChNFs. Among these methods, APS oxidation stands out as a cost-effective and eco-friendly approach that facilitates the efficient preparation of carboxylated ChNFs.

Seed nanopriming, an innovative agricultural nanotechnology, has demonstrated the potential to enhance seed

Nanotechnology and Biodelivery Laboratory, Department of Nutritional Sciences, University of Connecticut, Storrs, CT 06269, USA. E-mail: zhenlei.xiao@uconn.edu; yangchao.luo@uconn.edu; Fax: +1-860-486-3674; Tel: +1-860-486-2180; Web: <https://yangchao-luo.uconn.edu/>



performance by treating seeds with nanoparticles. This nanotechnology activates various physiological, biochemical, and signaling pathways during germination, leading to multiple benefits such as faster growth, improved seedling vigor, enhanced root and shoot development, increased plant yield and nutritional quality, and greater resistance to biotic and stress.^{11–13} For instance, nanopriming with CuO nanoparticles significantly improved the yield and biomass of broccoli and arugula,¹⁴ while selenium nanoparticles boosted growth, photosynthesis, nitrogen metabolism, and bioactive metabolite production in *Medicago interexta* sprouts.¹⁵

ChNFs hold great promise for seed nanopriming due to their nanoscale size, which enables them to cross biological barriers efficiently. Their negatively charged nanofibers could be readily absorbed by seeds.¹⁶ Additionally, the carbon-to-nitrogen ratio of chitin, typically ranging from 6 to 7, influences its decomposition rate and subsequent availability as a nitrogen source for plants.¹⁷

This study focuses on the sustainable extraction of chitin using DESs, followed by the preparation of ChNFs through APS oxidation. The effects of oxidation time on the structure, morphology, and functional properties of ChNFs were comprehensively investigated. Furthermore, the application of ChNFs as a seed nanopriming agent was explored, particularly in enhancing the growth of broccoli and radish seeds. Their impacts on seed germination, physiological characteristics, chlorophyll synthesis, nutrient contents, and antioxidant activity were evaluated. The findings provide valuable insights into the use of ChNFs for microgreen cultivation and contribute to the development of sustainable nanomaterials for agricultural enhancement.

2 Materials and methods

2.1 Materials

Lobster shells were kindly supplied by East Coast Seafood Company (New Bedford, MA, USA). 1,1-Diphenyl-2-picrylhydrazyl (DPPH) was obtained from Sigma-Aldrich (St. Louis, MO, USA). Choline chloride (99%), glycerol (99+%), lactic acid (analytical grade), ammonium persulfate (98+%), Trolox® (97%), rutin (95%), gallic acid (98%), 2,2'-azino-bis-(3-ethylbenzothiazoline-6-sulfonic acid) diammonium salt (ABTS) and other chemicals in analytical grade were obtained from Fisher Scientific Co. (Norcross, GA, USA).

2.2 Chitin extraction

The chitin extraction was conducted according to our previous paper.¹⁸ In detail, the lobster shell and choline chloride/lactic acid/glycerol deep eutectic solvent (CCLAGly) with a molar ratio of 1 : 1 : 1 were mixed at a mass ratio of 1 : 20 and heated at 50 °C for 2 h under magnetic stirring. The mixture was cooled to room temperature with the addition of distilled water. Then, it was filtered under vacuum, and the solids were washed with distilled water until reaching a neutral pH. Finally, the extracted chitin was dried overnight at 70 °C and stored in a desiccator for further use. The extracted chitin was designated as DES-Chitin.

2.3 Preparation of ChNFs

The method for preparing ChNFs from DES-Chitin was adapted and modified based on Ma *et al.*¹⁹ To be specific, the DES-Chitin (1 g) was added to 100 mL 2 N APS solution, and the mixture was heated at 70 °C for 3, 4, and 5 h. Then the water-insoluble fraction was filtered and washed repeatedly to neutral. Subsequently, the water-insoluble fraction of the APS-oxidized slurry was suspended in water at the concentration of 1 wt%, and the pH values were adjusted to 10 by the addition of sodium hydroxide solution (NaOH). Finally, ultrasonic treatment was applied to the suspension for 10 min using an ultrasonic liquid processor (Fisherbrand, FB-705, IL, USA) at 20 kHz and 700 W output powder. When the APS-oxidized slurry was ultrasonically treated at pH 10, transparent ChNF suspensions could be obtained. The prepared ChNFs with different oxidized time were named as 3h-ChNF, 4h-ChNF, and 5h-ChNF. The yield of prepared ChNFs was calculated based on eqn (1):

$$\text{Yield}(\%) = \frac{m_{\text{ChNFs}}}{m_{\text{DES-Chitin}}} \times 100\% \quad (1)$$

where m is the mass of the dried ChNFs and DES-Chitin (g), respectively.

2.4 Chemical, structure and morphology properties

2.4.1 Carboxyl content. The carboxyl contents (CC) of ChNFs were determined using the electrical potential titration method.¹⁰ ChNFs suspension (50 g) with a solid content of 0.1 wt% was adjusted to an electro potential of –220 mV using 0.1 M NaOH solution. Then, 0.01 M hydrochloric acid (HCl) was added to the suspension to increase the electro potential to 220 mV. CC (mmol g^{–1}) were calculated from the resulting electro potential curves based on the following eqn (2):

$$\text{CC} = \frac{(V_1 - V_2)C_{\text{HCl}}}{m_{\text{ChNFs}}} \quad (2)$$

where V_1 and V_2 are the amounts of HCl (mL) corresponding to the first and second equivalence points, C is the mol L^{–1} of HCl solution, and m is the mass of ChNFs (g).

2.4.2 Stability and transmittance of ChNFs suspensions. The stability of ChNF suspensions (0.1 wt% and 0.5 wt%) at pH 10 was evaluated by monitoring their transmittance over time after ultrasonic treatment. The transmittance measurements were performed using a Thermo Scientific spectrophotometer (Evolution 201, Madison, WI, USA), providing an indication of the dispersion stability of the suspensions.

2.4.3 Zeta potential. The Zeta potential of ChNFs was measured by using the nano ZetaSizer (Malvern Instruments Ltd, Worcestershire, UK). The zeta potential of ChNFs suspensions (0.1 wt%) was measured at pH from 3 to 11. The zeta potential was reported as an average of nine measurements.

2.4.4 Fourier transform infrared (FTIR) spectroscopy. The chemical structures were determined by FTIR spectroscopy. The FTIR spectra of DES-Chitin, and all prepared ChNFs were obtained using the Fisher Scientific Nicolet iS5 Spectrometer equipped with an iD7jATR accessory (Thermo Fisher Scientific



Inc., Waltham, MA, USA) within the wavenumber range of 500–400 cm^{-1} and analyzed by OMNIC software version 8.0.

2.4.5 Degree of acetylation (DA). DES-Chitin and all prepared ChNFs were loaded into a 4 mm Zirconia rotor, spun at 5 kHz, and analyzed using a Bruker AVANCE III 400 WB spectrometer. The instrument operated at frequencies of 400 MHz for ^1H and 100 MHz FOR ^{13}C . Data acquisition was performed with a 4 mm HXY CPMAS probe utilizing cross-polarization with total suppression of spinning sidebands (CPTOSS) for enhanced clarity. The measurements were conducted at 300 K with a 55 kHz decoupling field. The DAs of the samples were determined using the ratio of the integral (I) of methyl carbon atom of the *N*-acetyl group to the summation integrals of the six carbon atoms of the D -glucopyranosyl ring (C_1 – C_6 atoms) according to eqn (3):²⁰

$$\text{DA}(\%) = \frac{I_{\text{CH}_3}}{(I_{\text{C}_1} + I_{\text{C}_2} + I_{\text{C}_3} + I_{\text{C}_4} + I_{\text{C}_5} + I_{\text{C}_6})/6} \times 100 \quad (3)$$

2.4.6 Thermogravimetric analysis. The thermal stabilities of the DES-Chitin and all prepared ChNFs were determined using thermogravimetric analysis (TGA, TA instruments Q500–0188, USA).²¹ All samples with a weight of around 10 mg were held at 105 °C for 30 min to remove moisture and then heated to 700 °C at a heating rate of 10 °C min^{-1} under nitrogen. Data was recorded from 100 to 700 °C.

2.4.7 X-ray transform infrared spectroscopy (XRD). XRD analysis was performed on a Bruker D2 Phase Diffractometer (Bruker, Germany). The 2θ was in a range of 5–55° with a step size of 0.01° and 2 s per step as the counting time.¹ The crystallinity index (CrI; %) was calculated according to the following eqn (4):

$$\text{CrI}_{110} = \left[\frac{I_{110} - I_{\text{am}}}{I_{110}} \right] \times 100 \quad (4)$$

where I_{110} is the maximum intensity at $2\theta \cong 19^\circ$ and I_{am} is the intensity of amorphous diffraction at $2\theta \cong 12.6^\circ$.

2.4.8 Morphology observation. The morphology of prepared ChNFs was observed under atomic force microscopy (AFM, Tosca 200, Anton Paar, Graz, Austria). In brief, 5 μL of each ChNF suspension (0.001 wt%) was added to the Si-glass chip and air dried overnight at room temperature in a fume hood. After that, AFM imaging was performed using an AP-Arrow-NCR silicon cantilever in tapping mode with a resonance frequency of 285 kHz and a spring constant of 42 N m^{-1} . The scanning area was 5 $\mu\text{m} \times 5 \mu\text{m}$ for each sample, and all the samples were analyzed using Tosca Analysis software.

Transmission electron microscopy (TEM) was utilized to visualize the shape and morphology of freshly prepared ChNFs on the Tecnai T12 TEM (FEI, Hillsboro, Oregon, USA) as reported before.²² Briefly, 3 μL 0.001 wt% ChNF suspensions were added on a copper-coated 400 mesh grid and dried for 2 min, followed by staining of 0.5% uranyl acetate solution. After the sample was completely dried, the grid was loaded into the sample chamber of Tecnai T12 and the images were obtained by a CCD camera (AMT 2k XR40).

2.5 Broccoli and radish cultural and treatment

The cultivation of broccoli and radish was conducted randomly with 6 replications. These seeds were soaked in 5h-ChNF suspensions with different concentrations (10, 20, 30, 40, and 50 $\mu\text{g mL}^{-1}$ for broccoli seeds; 25, 50, 75, 100, and 200 $\mu\text{g mL}^{-1}$ for radish seeds) for 8 h in the dark, while control seeds were soaked in distilled water at pH 8 (0 $\mu\text{g mL}^{-1}$). To observe the germination, around 150 pretreated seeds were washed off 5h-ChNFs, and the seeds were uniformly spread on a seedling tray ($L \times W \times H$ 12 cm \times 8 cm \times 6 cm) containing a hydroponic grow mat in the greenhouse in the complete dark for the first three days, and the seed germination was checked when the germ length reached half of the seed length. Then, another 1.5 g pretreated seeds after germination were exposed to 12 h of daylight and 12 h of darkness per day, at 25 ± 2 °C, with $60 \pm 5\%$ relative humidity. The appropriate water was added per day. The seeds and seedlings were not completely submerged in the whole experiment. After a total of 13 days for broccoli and 10 days for radish growth, they were harvested. The root length and leaf area were calculated immediately and kept at -80 °C for further biochemical and molecular studies.

2.5.1 Growth parameters. The percentage of germinated seeds was calculated using a millimeter scale. Other growth parameters were evaluated by randomly selecting 20 roots and leaves from each tray. The length of seedlings was also measured using a millimeter scale. The leaf area was measured using ImageJ software (IJ 1.46r, Maryland, USA), while the weights of the fresh and freeze-dried microgreens were measured using an electronic analytical balance.

2.5.2 Elemental analysis. The total nitrogen (N) and carbon (C) contents in the broccoli and radish microgreens were determined by the Dumas method (AOAC 990.03) using a FlashSmart Elemental CHNS Analyzer (ThermoFisher Scientific Inc, USA).

2.5.3 Chlorophyll content. The measurement of photosynthetic pigment was done according to the Arno method, with some modification by using a Synergy H1 microplate reader (Bio Tek Instruments, Inc, Winooski, VT, USA). Briefly, 10 mg of freeze-dried leaves of broccoli and radish microgreens were extracted using 5 mL of 80% acetone. After 24 h in the dark, the samples were mixed for 3 min, and 200 μL of the extract was placed in each microplate cell. The absorption was recorded using the above microplate reader at wavelengths of 664, 645, and 470 nm. Finally, the amounts of chlorophyll *a*, chlorophyll *b*, and total chlorophyll were obtained in terms of mg/100 g dry weight using the eqn (5)–(7):^{23,24}

$$\text{Chlorophyll } a = \left(\frac{(12.7 \times A_{663}) - (2.69 \times A_{645})}{100 \times W} \right) \times V \quad (5)$$

$$\text{Chlorophyll } b = \left(\frac{(22.9 \times A_{645}) - (4.68 \times A_{663})}{100 \times W} \right) \times V \quad (6)$$

$$\text{Total chlorophyll} = \left(\frac{(20.08 \times A_{645}) - (8.02 \times A_{663})}{100 \times W} \right) \times V \quad (7)$$



where W is the sample weight (g), V is the 80% acetone solution volume (mL).

2.5.4 Nutrient analysis. A total of 10 mg of freeze-dried leaves were ground in 4 mL of PBS buffer (pH 7.4) and centrifuged at $12\,400\times g$ for 20 min at 4 °C. The resulting supernatant was collected for total soluble protein (TSP) quantification. The TSP content was determined using the Pierce BCA protein assay kit (Pierce, Rockford, IL), with bovine serum albumin (BSA) as the standard.¹⁸ Absorbance was measured at 562 nm, and the results were expressed as mg BSA equivalent (BSAE) per gram of dried weight (DW).

For polyphenol and flavonoid analysis, 20 mg of freeze-dried leaves were extracted with 5 mL of 70% ethanol and subjected to sonication for 1 h twice. The ethanol extract was then used for further analysis.

Total polyphenol content (TPC) was measured using a modified version of our previous method.²⁵ Briefly, 0.2 mL of the ethanol extract was mixed with 1 mL of the Folin-Ciocalteu phenol reagent in plastic test tubes. After 5 min, 0.8 mL of 7.5% sodium carbonate was added, and the mixture was incubated at room temperature for 1 h. The absorbance was measured at 765 nm, with gallic acid used as the standard for calibration. The results were expressed as mg gallic acid equivalent (GAE) per gram of DW.

Total flavonoid content (TFC) was determined using the aluminum chloride method as previously described.²⁶ In brief, 1 mL of the ethanol extract was mixed with 4 mL of distilled water and 0.3 mL of 5% sodium nitrate in plastic test tubes. After 6 min, 0.3 mL of 10% aluminum chloride was added, followed by another 6 min incubation. Subsequently, 2 mL of 1 mol L⁻¹ sodium hydroxide was added, and the final volume was adjusted to 10 mL with distilled water. The mixture was incubated in the dark at room temperature for 15 min, and absorbance was recorded at 415 nm. The TFC content was determined using a rutin calibration curve and expressed as mg rutin equivalent (RE) per gram of DW.

2.5.5 Antioxidant activity. The antioxidant activity was assessed using DPPH and ABTS radical scavenging assays, following our previous methods with slight modifications.²⁷

For the DPPH assay, 1 mL of the ethanol extract was mixed with 2 mL of DPPH solution and incubated in the dark at room temperature for 30 minutes. The absorbance was then measured at 571 nm. The antioxidant activity was quantified using a Trolox® calibration curve and expressed as mmol Trolox® equivalent (TE) per gram of DW.

For the ABTS assay, 1 mL of the ethanol extract was combined with 2 mL of ABTS solution and incubated at room temperature for 6 minutes. The absorbance was recorded at 734 nm. Similarly, the antioxidant activity was calculated based on a Trolox® calibration curve and expressed as mmol TE per gram of DW.

2.6 Statistical analysis

All statistical analyses were performed using IBM SPSS Statistics for Windows version 23.0 (SPSS Inc., USA). One-way ANOVA followed by the Duncan test was performed to determine the

significance of difference at $P < 0.05$ among tested groups. All experiments were conducted in triplicate unless otherwise stated.

3 Results and discussion

3.1 Characterization of ChNFs

3.1.1 Extraction of chitin with DESs and ChNFs preparation. The extraction process of chitin using DESs was illustrated in Fig. 1a. Lactic acid served as a hydrogen ion donor, facilitating the removal of calcium carbonate from lobster shells. This demineralization disrupted the structural integrity of the chitin-protein matrix, increasing the spatial separation of the matrix. Proteins are rich in carboxyl and hydroxyl groups, acting as hydrogen bond donors that compete with chloride anions *via* electrostatic interaction in the DES system. Consequently, the formation of new hydrogen bonds between protein and choline chloride could disrupt the hydrogen bonds within the chitin-protein matrix. As a result, DES-chitin with a yield of $26.22 \pm 2.14\%$ and a purity of $94.78 \pm 0.39\%$ was obtained, which was comparable to chemically extracted chitin.

DES-Chitin was subsequently subjected to APS oxidation to produce ChNFs. During this process, amorphous regions were removed, and hydroxyl groups at the C₆ position were oxidized into carboxyl groups (Fig. 1b). The principal mechanism could be that free radicals generated by APS, including (SO₄)⁻, H₂O₂, and HSO₄⁻ facilitated the breakdown of amorphous regions.^{28,29} As shown in Fig. 1c, extending oxidation time from 3 h to 5 h resulted in a significantly decreased yield from 71.83% to 63.92% ($P < 0.05$), attributed to further dissolution of amorphous regions and thus lower yield.

3.1.2 Crystallinity and degree of acetylation. The XRD patterns of DES-Chitin and prepared ChNFs, as shown in Fig. 2a, revealed characteristic diffraction peaks at $2\theta = 9.2^\circ$ (020), 12.65° (021), 19.2° (110), 23.41° (130), and 26.29° (013). These peaks confirmed the presence of the stable α -chitin crystalline structure. Based on eqn (4), the CrI values of DES-Chitin, 3h-ChNF, 4h-ChNF, and 5h-ChNF were 77.87%, 81.25%, 84.53%, and 88%, respectively, indicating a progressive increase in crystallinity with extended oxidation time. This trend corresponded with the observed yield results, as the amorphous regions in DES-Chitin were gradually removed by APS treatment, enhancing the overall crystallinity. Similar findings were reported by other researchers,³⁰ where the CrI of chitin nanocrystals prepared using the APS method increased from 86.2% to 93.5%. Their study also demonstrated that chitin nanocrystals exhibited sharper and more intense XRD peaks than native chitin, attributed to the elimination of amorphous regions and the resulting improvement in crystallinity. These observations were consistent with the current results, reinforcing the role of APS treatment in enhancing nano chitin crystallinity.

The DA is a crucial parameter for distinguishing chitin from chitosan, with values above 50% classifying the polymer as chitin. In this study, the DA of all samples was determined using ¹³C solid-state NMR spectroscopy. The spectra for DES-Chitin and the prepared ChNFs were presented in Fig. 2b. The





Fig. 1 (a) Process of DES extracted chitin from lobster shells;¹⁸ (b) preparation of ChNFs after APS oxidation;³⁰ (c) yields of 3h-ChNF, 4h-ChNF, and 5h-ChNF. Different lower-case letters indicate significant differences among groups ($P < 0.05$).

characteristic chemical shifts were observed at 104.76 (C_1), 55.89 (C_2), 74.06 (C_3), 84.11 (C_4), 76.47 (C_5), 61.65 (C_6), 174.65 ($C=O$), and 23.52 (CH_3) ppm. Based on Fig. 2b and eqn (3), the DA values of DES-Chitin, 3h-ChNF, 4h-ChNF, and 5h-ChNF were

calculated to be 96%, 96.27%, 96.54%, and 96.28%, respectively. These results demonstrated that the DA values remained consistent across all samples, with minimal variation. This stability could be attributed to the absence of alkaline treatment

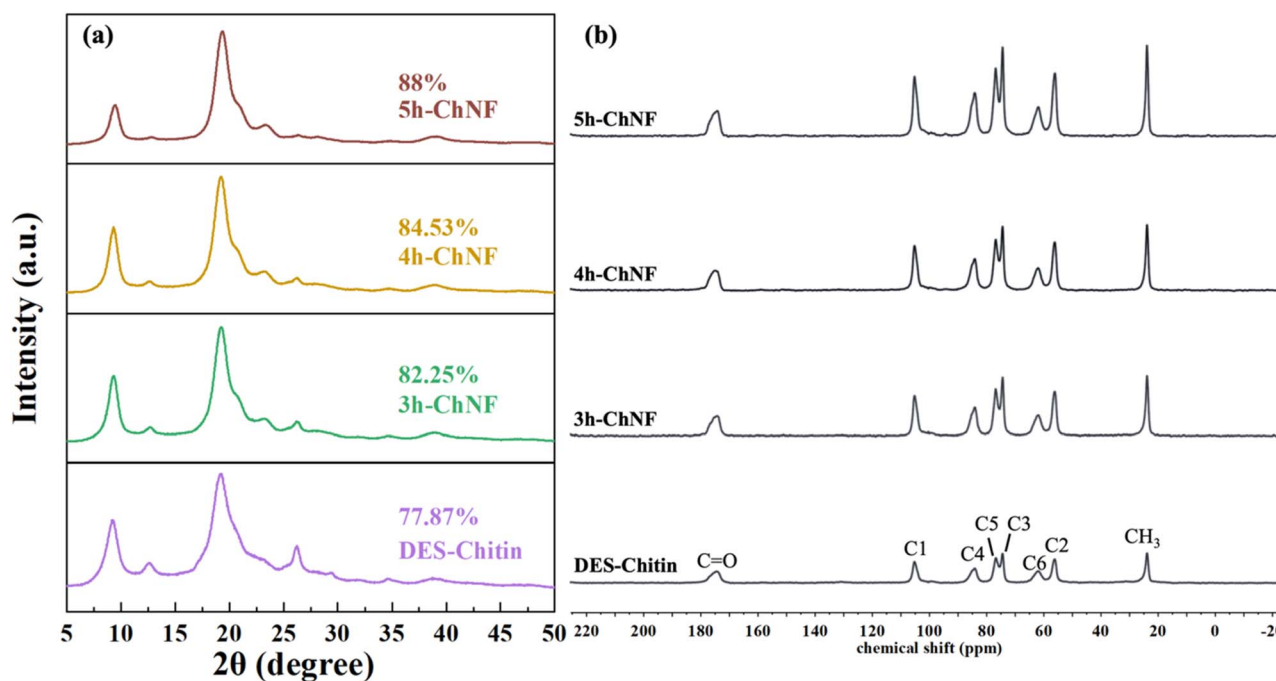


Fig. 2 (a) XRD spectra of DES-Chitin, 3h-ChNF, 4h-ChNF, and 5h-ChNF, with their respective crystallinity index shown above each spectrum; (b) ^{13}C solid-state NMR spectra of DES-Chitin, 3h-ChNF, 4h-ChNF, and 5h-ChNF.



in the preparation process, which is known to induce deacetylation. For comparison, Tanpichai and coworkers²⁰ treated ChNFs with 30% NaOH for 120, 240, and 480 minutes, reporting significant reductions in DA values with increasing treatment duration. Interestingly, the ¹³C NMR spectral profiles of all the samples in this study were essentially identical. Similar observations were reported by others¹⁹ for purified β -chitin and β -ChNFs, revealing that the conversion of $-\text{CH}_2\text{OH}$ to $-\text{COOH}$ did not have an obvious effect on the chemical shift of the carbon atom attached to the NH_2 .

3.1.3 Determination and characterization of carboxylic groups. The carboxylic content of prepared ChNFs was measured using the electrical potential titration method. As shown in Fig. 3a, the carboxyl contents for 3h-ChNF, 4h-ChNF, and 5h-ChNF were determined to be $0.24 \pm 0.07 \text{ mmol g}^{-1}$, $0.53 \pm 0.01 \text{ mmol g}^{-1}$, and $0.73 \pm 0.08 \text{ mmol g}^{-1}$, respectively. Similar findings were reported by Zhang *et al.*,³¹ who observed an increase in carboxyl content from 0.56 mmol g^{-1} to 0.99 mmol g^{-1} as the APS concentration rose during the preparation of cellulose nanocrystals. Likewise, Ma *et al.*¹⁹ optimized APS oxidation conditions for ChNFs synthesis and achieved carboxyl content up to 0.8 mmol g^{-1} .

The carboxyl content of ChNFs plays a critical role in their dispersion, particularly in alkaline solutions. As illustrated in Fig. 3b, the transmittances of 0.1 wt% and 0.5 wt% in distilled water at pH 10 were evaluated. At a concentration of 0.1 wt%, all ChNFs exhibited high transparency, with transmittance exceeding 95% at 800 nm. However, at 0.5 wt%, the transmittance of 3h-ChNF dropped significantly to 72.7%, while 4h-

ChNF maintained a slightly reduced transmittance of 94.7%. Notably, 5h-ChNF at 0.5 wt% remained highly transparent, with transmittance reaching 97.8%, surpassing even that of 0.1 wt% 3h-ChNF. Wang *et al.*³² also reported that prolonged treatment reduced the size of ChNFs, resulting in improved transparency. According to light scattering theory, when the diameter of ChNFs is significantly smaller than the wavelength of incident light, scattering becomes isotropic. Consequently, smaller ChNFs diameters, relative to visible light wavelengths, contribute to high optical transparency in suspensions.³³ Besides, under alkaline conditions, carboxyl groups are ionized into negatively charged carboxylate ions. Increased carboxyl content enhanced this ionization, amplifying electrostatic repulsion between nanofibers and minimizing aggregation, resulting in a more homogeneous and transparent solution.

The zeta potential, representing the potential difference between the dispersion medium and the stationary layer surrounding dispersed ChNFs, provides insight into ChNF stability within a suspension. A zeta potential of at least -30 mV is generally required for electrostatically stabilized systems to ensure physical stability.³⁴ Fig. 3c showed the zeta potential of ChNF suspensions across a pH range of 3 to 11. Only 3h-ChNF maintained a zeta potential above -30 mV at pH 7–11. Conversely, 4h-ChNF and 5h-ChNF displayed zeta potentials below -30 mV , indicating better dispersibility in neutral and basic conditions due to the presence of increased anionic COO^- groups. These observations aligned with the trends in carboxyl content and transmittance, reinforcing the link between surface charge, electrostatic interactions, and dispersion stability.



Fig. 3 (a) Carboxyl contents of 3h-ChNF, 4h-ChNF, and 5h-ChNF suspensions; (b) UV spectra, inserted photos show the suspensions transparency; (c) zeta potential of 3h-ChNF, 4h-ChNF, and 5h-ChNF suspensions across a pH range of 3 to 11; (d) FTIR spectra of DES-Chitin, 3h-ChNF, 4h-ChNF, and 5h-ChNF. Different lower-case letters indicate significant differences among groups ($P < 0.05$).



FTIR analysis was conducted to examine chemical structure changes in DES-Chitin and the prepared ChNFs. As shown in Fig. 3d, characteristic peaks were observed for all samples, including 3444 cm^{-1} (O–H stretching), 3257 cm^{-1} and 3103 cm^{-1} (N–H stretching), 1655 cm^{-1} and 1621 cm^{-1} (amide I), 1552 cm^{-1} (amide II), and 1311 cm^{-1} (amide III).^{3,18} Notably, the absorption peak for carboxyl groups in the prepared ChNFs was not significant, likely due to hydrogen bonding between carboxyl and amide groups in the dry infrared samples.¹⁰ However, a minor peak at 1734 cm^{-1} , corresponding to free carboxyl groups, was detected in 5h-ChNF as oxidation time increased, consistent with prior findings by Fan *et al.*³⁵ This subtle change supported the conclusions that extended oxidation promoted the conversion of carboxyl groups in DES-Chitin.

3.1.4 Morphology of ChNF. The morphology of 3h-ChNF, 4h-ChNF, and 5h-ChNF, prepared by APS oxidation of DES-Chitin in aqueous solution at pH 10, was examined using AFM (Fig. 4a–c) and TEM (Fig. 4d–f). All ChNFs exhibited a needle-like structure, resembling the morphology of chitin nanocrystals produced *via* APS oxidation, as reported.³⁰ Statistical analysis of the TEM images by using ImageJ software revealed (Fig. 4g and h) that the average length and width of 3h-ChNF were $331 \pm 59\text{ nm}$ and $17 \pm 4\text{ nm}$, respectively. For 4h-ChNF, these dimensions decreased to $201 \pm 55\text{ nm}$ in length and $12 \pm 2\text{ nm}$ in width, while 5h-ChNF showed further reductions to $172 \pm 48\text{ nm}$ in length and $9 \pm 3\text{ nm}$ in width. This progressive decrease in both length and width with increasing oxidation time also aligned with the transmittance results, further highlighting the relationship between oxidation time and nanofiber size reduction.

3.1.5 Thermal stability. The thermal stability of DES-Chitin and the prepared ChNFs was analyzed using TGA. The results are shown in Fig. 5. The TGA curves of all samples revealed two distinct weight loss stages. The first stage, occurring before

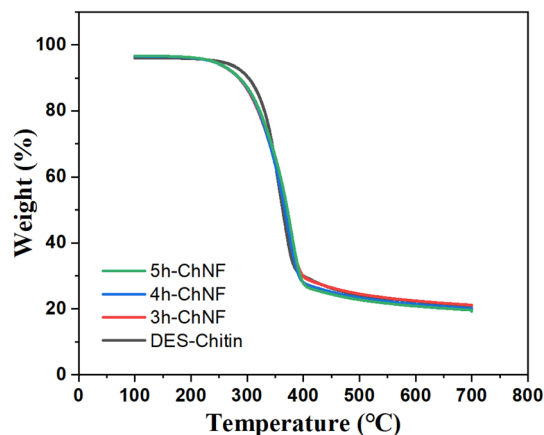


Fig. 5 TGA profiles of DES-Chitin, 3h-ChNF, 4h-ChNF and 5h-ChNF.

200 °C, corresponded to the evaporation of water.¹⁸ In this stage, the weight loss of DES-Chitin and 3h-ChNF, 4h-ChNF, and 4h-ChNF was 4.2%, 3.82%, 3.93%, and 3.81%, respectively, with no significant differences observed among the samples. The second weight loss stage, between 200 °C and 400 °C, was ascribed to the dehydration of saccharide rings and the degradation of acetylated chitin units.³⁶ The total weight loss of DES-Chitin and 3h-ChNF, 4h-ChNF, and 4h-ChNF was 70.06%, 70.14%, 71.94%, and 72.14%, respectively. Again, no significant differences were observed, indicating that the thermal stability of the prepared ChNFs was comparable to that of DES-Chitin. Yuan *et al.*³⁷ also found that the thermal stability of chitin nanocrystals was similar to that of pristine chitin.

3.2 Seed germination and growth

The effectiveness of seed nanoprimering is primarily due to the distinctive properties of nanomaterials. Their smaller size

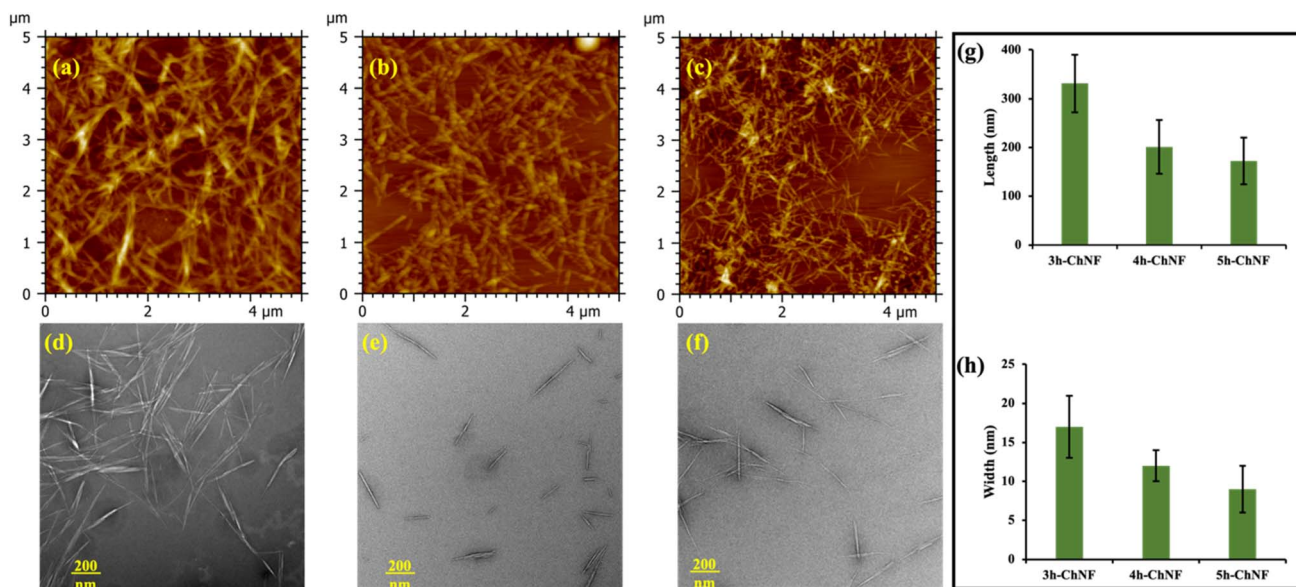


Fig. 4 AFM and TEM images of 3h-ChNF (a and d), 4h-ChNF (b and e), and 5h-ChNF (c and f), as well as the calculated Length (g) and width (h).





Fig. 6 Photographs of broccoli (a) and radish (b) growth after different days, and effects of 5h-ChNF on leaf area and root length of broccoli (c) and radish (d) when harvested.

allows them to penetrate biological barriers more efficiently, while their charged nature facilitates uptake by plants.³⁸ Based on the above hypothetical reasons, 5h-ChNF was chosen for further evaluation. As shown in Fig. 6, broccoli and radish seeds treated with 5h-ChNF exhibited notable growth improvement after three days of germination. Following exposure to light and hydroponic cultivation, the seedlings turned green, with those treated with 5h-ChNF showing better growth compared to the control group. Enhanced leaf area and root length were observed in the treated seedlings, with detailed growth parameters provided in the subsequent sections (Tables 1 and 2).

3.2.1 Effect of ChNFs on physiological characteristics. To evaluate the potential of 5-ChNF as a seed nanoprimer agent for microgreens, its effects on broccoli and radish seedlings were assessed by analyzing germination rates, root length, fresh and dry weights, and leaf area at varying concentrations. Results revealed a concentration-dependent response, with specific concentrations promoting optimal growth for each microgreen species.

For broccoli microgreens, the application of 5h-ChNF at 20 $\mu\text{g mL}^{-1}$ yielded the most notable growth improvements. The germination rate rose to $89.38 \pm 2.92\%$, significantly ($P < 0.05$) higher than the control group ($79.39 \pm 0.75\%$). At this optimal concentration, root length and leaf area peaked at 4.10 ± 0.10 cm and 0.42 ± 0.04 cm², respectively. Fresh weight increased to 14.08 ± 0.66 g, while dry weight reached 1.08 ± 0.04 g, indicating remarkably enhanced biomass accumulation. However, concentrations exceeding $20 \mu\text{g mL}^{-1}$ failed to provide further benefits and, in some cases, resulted in slight declines, suggesting a threshold for the stimulatory effects.

Similarly, radish microgreens demonstrated optimal growth at a higher concentration of $75 \mu\text{g mL}^{-1}$. At this level, the germination rate increased to $97.82 \pm 2.00\%$, while root length reached 5.22 ± 0.22 cm. Fresh and dry weights were also maximized at 17.38 ± 0.12 g and 1.5 ± 0.02 g, respectively. Leaf area exhibited a significant increase ($P < 0.05$), rising from 1.05 ± 0.13 cm² in the control group to 1.46 ± 0.12 cm². Notably, radish seedlings displayed higher tolerance to elevated concentrations of 5h-ChNF, with no adverse effects observed up



Table 1 Effects of 5h-ChNF on growth in broccoli and radish microgreens^a

Broccoli	0 ($\mu\text{g mL}^{-1}$)	10 ($\mu\text{g mL}^{-1}$)	20 ($\mu\text{g mL}^{-1}$)	30 ($\mu\text{g mL}^{-1}$)	40 ($\mu\text{g mL}^{-1}$)	50 ($\mu\text{g mL}^{-1}$)
Germination rate (%)	79.39 \pm 0.75 ^c	83.68 \pm 2.75 ^b	89.38 \pm 2.92 ^a	84.14 \pm 2.99 ^b	84.49 \pm 0.77 ^b	85.82 \pm 0.74 ^{ab}
Root length (cm)	3.62 \pm 0.28 ^b	3.94 \pm 0.23 ^a	4.10 \pm 0.10 ^a	4.01 \pm 0.38 ^a	4.00 \pm 0.10 ^a	3.98 \pm 0.09 ^a
Fresh weigh (g)	11.29 \pm 1.25 ^c	13.16 \pm 0.59 ^b	14.80 \pm 0.66 ^a	13.36 \pm 0.82 ^b	11.75 \pm 0.55 ^c	14.02 \pm 0.70 ^{ab}
Dry weight (g)	0.96 \pm 0.07 ^b	1.00 \pm 0.05 ^{ab}	1.08 \pm 0.04 ^a	1.05 \pm 0.06 ^a	1.02 \pm 0.04 ^{ab}	1.01 \pm 0.01 ^{ab}
Leaf area (cm ²)	0.33 \pm 0.04 ^c	0.39 \pm 0.04 ^b	0.42 \pm 0.04 ^a	0.41 \pm 0.04 ^{ab}	0.39 \pm 0.02 ^b	0.41 \pm 0.03 ^{ab}
Radish	0 ($\mu\text{g mL}^{-1}$)	25 ($\mu\text{g mL}^{-1}$)	50 ($\mu\text{g mL}^{-1}$)	75 ($\mu\text{g mL}^{-1}$)	100 ($\mu\text{g mL}^{-1}$)	200 ($\mu\text{g mL}^{-1}$)
Germination rate (%)	93.57 \pm 3.25 ^a	95.03 \pm 1.34 ^a	95.19 \pm 2.95 ^a	97.82 \pm 2.00 ^a	96.85 \pm 0.88 ^a	97.49 \pm 2.18 ^a
Root length (cm)	4.57 \pm 0.27 ^b	5.08 \pm 0.42 ^a	5.12 \pm 0.36 ^a	5.22 \pm 0.22 ^a	5.19 \pm 0.14 ^a	5.14 \pm 0.40 ^a
Fresh weigh (g)	17.18 \pm 0.47 ^a	17.19 \pm 0.57 ^a	17.28 \pm 1.02 ^a	17.38 \pm 0.12 ^a	17.09 \pm 1.6 ^a	17.27 \pm 0.89 ^a
Dry weight (g)	1.39 \pm 0.04 ^b	1.40 \pm 0.03 ^b	1.44 \pm 0.03 ^{ab}	1.50 \pm 0.02 ^a	1.45 \pm 0.04 ^{ab}	1.49 \pm 0.07 ^a
Leaf area (cm ²)	1.05 \pm 0.13 ^c	1.26 \pm 0.13 ^b	1.24 \pm 0.06 ^b	1.46 \pm 0.12 ^a	1.40 \pm 0.17 ^a	1.41 \pm 0.11 ^a

^a Different lower-case letters indicate significant differences among various concentration groups for each parameter within the same microgreens ($P < 0.05$).

to 75 $\mu\text{g mL}^{-1}$. Beyond this concentration, similar to broccoli, growth improvements plateaued or slightly declined.

These observations aligned with previous findings that natural oligosaccharides and polysaccharides exhibited positive physiological effects at low concentrations, while higher concentrations can lead to inhibitory activity.^{39–41} For example, Li *et al.*⁴² found that high concentrations (100 $\mu\text{g mL}^{-1}$) of chitosan nanoparticles inhibited wheat seedling growth, likely due to induced cellular stress or apoptosis.

3.2.2 Effect of ChNFs on nitrogen and chlorophyll contents. The impacts of 5h-ChNF on nitrogen, carbon, and chlorophyll contents in broccoli and radish microgreens were systematically assessed. The results revealed that appropriate concentrations of 5h-ChNF significantly enhanced nitrogen assimilation, which in turn promoted chlorophyll synthesis, while the carbon content remained relatively stable.

For broccoli microgreens, the nitrogen content increased markedly ($P < 0.05$) from 3.58 \pm 0.07% in the control group to a peak of 5.35 \pm 0.29% at 20 $\mu\text{g mL}^{-1}$ of 5h-ChNF. A similar

trend was observed for radish microgreens, where nitrogen levels rose from 3.82 \pm 0.80% in the control group to a maximum of 5.31 \pm 0.35% at 75 $\mu\text{g mL}^{-1}$. Beyond these optimal concentrations, nitrogen levels showed slight declines, indicating that excessive application may inhibit further nitrogen assimilation. In contrast, the carbon content in both broccoli and radish remained relatively consistent ($P > 0.05$), ranging from 43.28 \pm 0.10% to 45.59 \pm 0.63% for broccoli and 43.23 \pm 0.69 to 44.11 \pm 0.16% for radish, suggesting that 5h-ChNF primarily influenced nitrogen metabolism over carbon metabolism. These findings were consistent with prior research. Cheng *et al.*⁴³ reported that nanochitin whiskers enhanced nitrogen metabolism more effectively than carbon metabolism, resulting in increased nitrogen accumulation and grain yield in winter wheat. Likewise, Zhan and coworkers⁴⁴ demonstrated that chitin significantly improved nitrogen uptake efficiency in pomelo orchards.

Nitrogen availability is directly correlated with chlorophyll contents, as nitrogen is a critical component of the chlorophyll

Table 2 Effects of 5h-ChNF on nitrogen, carbon, and chlorophyll contents in broccoli and radish microgreens^a

Broccoli	0 ($\mu\text{g mL}^{-1}$)	10 ($\mu\text{g mL}^{-1}$)	20 ($\mu\text{g mL}^{-1}$)	30 ($\mu\text{g mL}^{-1}$)	40 ($\mu\text{g mL}^{-1}$)	50 ($\mu\text{g mL}^{-1}$)
Nitrogen (%)	3.58 \pm 0.07 ^c	4.30 \pm 0.28 ^{bc}	5.35 \pm 0.29 ^a	4.79 \pm 0.22 ^{ab}	4.62 \pm 0.59 ^{ab}	4.69 \pm 1.29 ^{ab}
Carbon (%)	43.28 \pm 0.10 ^c	44.08 \pm 0.34 ^b	45.58 \pm 0.63 ^a	44.52 \pm 0.34 ^b	44.31 \pm 0.29 ^b	44.20 \pm 0.51 ^b
Chlorophyll <i>a</i> (mg/100 g)	26.52 \pm 0.35 ^d	29.87 \pm 0.56 ^c	35.64 \pm 1.12 ^a	33.84 \pm 2.12 ^a	31.13 \pm 0.22 ^{bc}	33.39 \pm 2.21 ^{ab}
Chlorophyll <i>b</i> (mg/100 g)	9.52 \pm 0.45 ^c	11.03 \pm 0.52 ^b	13.20 \pm 0.77 ^a	12.28 \pm 0.84 ^{ab}	11.90 \pm 0.32 ^b	12.25 \pm 1.43 ^{ab}
Total chlorophyll (mg/100 g)	36.12 \pm 0.61 ^c	40.20 \pm 1.46 ^b	48.68 \pm 1.94 ^a	46.09 \pm 1.77 ^a	43.03 \pm 0.37 ^b	45.96 \pm 3.23 ^a
Radish	0 ($\mu\text{g mL}^{-1}$)	25 ($\mu\text{g mL}^{-1}$)	50 ($\mu\text{g mL}^{-1}$)	75 ($\mu\text{g mL}^{-1}$)	100 ($\mu\text{g mL}^{-1}$)	200 ($\mu\text{g mL}^{-1}$)
Nitrogen (%)	3.82 \pm 0.80 ^b	4.61 \pm 0.11 ^{ab}	4.59 \pm 0.40 ^{ab}	5.31 \pm 0.35 ^a	5.00 \pm 0.33 ^{ab}	5.20 \pm 0.97 ^a
Carbon (%)	43.23 \pm 0.69 ^a	43.91 \pm 0.72 ^a	43.67 \pm 0.58 ^a	44.11 \pm 0.16 ^a	43.86 \pm 0.02 ^a	43.95 \pm 0.67 ^a
Chlorophyll <i>a</i> (mg/100 g)	13.50 \pm 0.62 ^d	17.18 \pm 0.85 ^c	24.83 \pm 1.18 ^b	29.11 \pm 2.01 ^a	29.73 \pm 2.74 ^a	28.47 \pm 1.29 ^a
Chlorophyll <i>b</i> (mg/100 g)	4.93 \pm 0.87 ^b	5.72 \pm 0.15 ^b	6.36 \pm 1.38 ^b	9.75 \pm 0.26 ^a	9.36 \pm 1.32 ^a	9.29 \pm 0.66 ^a
Total chlorophyll (mg/100 g)	17.87 \pm 0.04 ^d	22.63 \pm 1.17 ^c	31.55 \pm 1.23 ^b	38.92 \pm 2.15 ^a	38.82 \pm 2.54 ^a	37.61 \pm 2.12 ^a

^a Different lower-case letters indicate significant differences among groups ($P < 0.05$).



molecule, essential for photosynthesis.⁴⁵ As shown in Table 2, in broccoli, increasing the concentration of 5h-ChNF from 0 to 20 $\mu\text{g mL}^{-1}$ improved chlorophyll *a*, chlorophyll *b*, and total chlorophyll contents from 26.52 ± 0.35 mg/100 g, 9.52 ± 0.45 mg/100 g and 36.12 ± 0.61 mg/100 g to 35.64 ± 1.12 mg/100 g, 13.20 ± 0.77 mg/100 g, and 48.68 ± 1.94 mg/100 g, respectively. Similarly, in radish, chlorophyll *a*, chlorophyll *b* and total chlorophyll contents peaked at 29.11 ± 2.01 mg/100 g, 9.75 ± 0.26 mg/100 g, and 38.92 ± 2.15 mg/100 g at 75 $\mu\text{g mL}^{-1}$ of 5h-ChNF. These results were in line with the previous studies on the role of nitrogen in chlorophyll synthesis. Wu *et al.*⁴⁶ found that nitrogen-rich conditions maximized chlorophyll contents in *Larix olgensis* seedlings. In detail, when supplied with 8 mmol L^{-1} nitrate, the contents of chlorophyll reached a maximum. However, a continuous increase in nitrate concentration induced a slight decrease in chlorophyll contents, which could be explained by the chlorophyll biosynthesis mechanism. It is well-known that the chlorophyll molecule contains four pyrrole rings, and their synthesis, along with their binding to magnesium ions, requires substantial nitrogen inputs.^{47,48} Nitrogen deficiency will lead to chloroplast disassembly and shifts in signaling pathways, affecting stress responses and source-sink dynamics essential for crop yield optimization.⁴⁹ Conversely, excessive nitrogen accumulation may disturb the balance of carbon and nitrogen within plants, resulting in metabolic imbalances that compromise plant health and reduce yield potential.⁵⁰

3.2.3 Nutrient analysis. The nutrient contents, including protein, polyphenols, and flavonoids, in broccoli and radish microgreens were further analyzed to assess the impact of varying concentrations of 5h-ChNF (Table 3).

For broccoli microgreens, protein content increased significantly ($P < 0.05$) from 246.61 ± 8.23 mg BSAE/g DW in the control group to a peak of 285.85 ± 9.65 mg BSAE/g DW at 20 $\mu\text{g mL}^{-1}$ of 5h-ChNF. However, at higher concentrations (30–50 $\mu\text{g mL}^{-1}$), protein contents slightly decreased, though still remaining higher than the control ($P > 0.05$). This trend was consistent with the nitrogen content results shown in Table 2. A similar pattern was observed for polyphenols and flavonoids. Polyphenol levels significantly ($P < 0.05$) increased from 44.99 ± 92.63 mg GAE/g DW in the control group to 51.79 ± 1.57 mg

GAE/g DW. However, at higher concentrations, polyphenol content showed a slight decline, which was not statistically significant ($P > 0.05$). Flavonoid content also reached its peak at 20 $\mu\text{g mL}^{-1}$, with a value of 110.21 ± 4.33 mg RE/g DW. These findings suggested that optimal nitrogen availability promoted secondary metabolite biosynthesis, but excessive nitrogen may disrupt the balance between primary and secondary metabolism, leading to reduced polyphenol and flavonoid production.^{51,52} In radish microgreens, protein content significantly increased ($P < 0.05$) from 263.33 ± 14.41 mg BSAE/g DW in the control to 299.69 ± 5.38 mg BSAE/g DW at 75 $\mu\text{g mL}^{-1}$, with no significant reduction at higher concentrations ($P > 0.05$). Unlike in broccoli, where excessive 5h-ChNF negatively impacted bioactive compound levels, radish microgreens maintained relatively stable polyphenol and flavonoid contents across all treatments, suggesting that radish microgreens may tolerate higher levels of 5h-ChNF. Therefore, further investigation into the differences in nitrogen metabolism between these two microgreen species is warranted to better understand their distinct responses.

3.2.4 Antioxidant activity. The antioxidant activity of microgreen leaves, assessed by DPPH and ABTS assays, further highlighted the difference in response to varying concentrations of 5h-ChNF between broccoli and radish microgreens, as summarized in Table 4.

In broccoli microgreens, DPPH radical scavenging activity showed a significant increase ($P < 0.05$) compared with the control group (3.49 ± 0.10 mmol TE g^{-1} DW), peaking at 4.16 ± 0.48 mmol TE g^{-1} DW at 20 $\mu\text{g mL}^{-1}$, after which no further significant changes were observed at higher concentrations ($P > 0.05$). Similarly, ABTS activity significantly ($P < 0.05$) increased from 7.88 ± 0.18 mmol TE g^{-1} DW in the control to 8.09 ± 0.01 mmol TE g^{-1} DW at 20 $\mu\text{g mL}^{-1}$, remaining stable at higher concentrations.

In radish microgreens, DPPH antioxidant activity was also significantly higher ($P < 0.05$) than the control (2.74 ± 0.11 mmol TE g^{-1} DW), reaching a peak at 3.35 ± 0.04 mmol TE g^{-1} DW at 75 $\mu\text{g mL}^{-1}$, and remaining stable at higher concentrations. A similar trend was observed in the ABTS assay, where antioxidant activity significantly increased ($P < 0.05$) from 6.98 ± 0.33 mmol TE g^{-1} DW to 7.69 ± 0.24 mmol TE g^{-1} DW at 75

Table 3 Effects of 5h-ChNF on nutrient contents^a

Broccoli	0 ($\mu\text{g mL}^{-1}$)	10 ($\mu\text{g mL}^{-1}$)	20 ($\mu\text{g mL}^{-1}$)	30 ($\mu\text{g mL}^{-1}$)	40 ($\mu\text{g mL}^{-1}$)	50 ($\mu\text{g mL}^{-1}$)
Protein (mg BSAE/g DW)	246.61 ± 8.23^b	248.12 ± 12.89^b	285.85 ± 9.65^a	271.56 ± 12.80^{ab}	265.23 ± 11.84^{ab}	275.27 ± 14.93^a
Polyphenol (mg GAE/g DW)	44.99 ± 2.63^c	45.76 ± 3.05^{bc}	51.79 ± 1.57^a	48.62 ± 2.04^{abc}	49.45 ± 4.02^{abc}	49.97 ± 0.78^{ab}
Flavonoid (mg RE/g DW)	87.38 ± 4.48^c	88.94 ± 2.24^c	110.21 ± 4.33^a	93.58 ± 4.06^{bc}	93.05 ± 1.31^{bc}	97.18 ± 1.83^b
Radish	0 ($\mu\text{g mL}^{-1}$)	25 ($\mu\text{g mL}^{-1}$)	50 ($\mu\text{g mL}^{-1}$)	75 ($\mu\text{g mL}^{-1}$)	100 ($\mu\text{g mL}^{-1}$)	200 ($\mu\text{g mL}^{-1}$)
Protein (mg BSAE/g DW)	263.33 ± 14.41^c	273.05 ± 13.56^{bc}	279.32 ± 17.23^{abc}	299.69 ± 5.38^a	287.08 ± 11.49^{ab}	296.57 ± 8.92^a
Polyphenol (mg GAE/g DW)	46.09 ± 0.95^b	48.55 ± 2.70^{ab}	48.34 ± 4.65^b	53.42 ± 3.93^a	50.47 ± 0.93^{ab}	51.01 ± 1.60^{ab}
Flavonoid (mg RE/g DW)	48.08 ± 0.44^b	52.92 ± 1.66^{ab}	55.69 ± 2.64^a	57.03 ± 0.04^a	57.47 ± 2.04^a	55.27 ± 5.40^a

^a Different lower-case letters indicate significant differences among groups ($P < 0.05$).



Table 4 Antioxidant activity of microgreen leaves determined by the DPPH and ABTS assays^a

Broccoli	0 ($\mu\text{g mL}^{-1}$)	10 ($\mu\text{g mL}^{-1}$)	20 ($\mu\text{g mL}^{-1}$)	30 ($\mu\text{g mL}^{-1}$)	40 ($\mu\text{g mL}^{-1}$)	50 ($\mu\text{g mL}^{-1}$)
DPPH (mmol TE g^{-1} DW)	3.49 ± 0.10^b	3.84 ± 0.19^{ab}	4.16 ± 0.48^a	4.08 ± 0.38^{ab}	4.02 ± 0.38^{ab}	4.04 ± 0.23^{ab}
ABTS (mmol TE g^{-1} DW)	7.88 ± 0.18^b	7.89 ± 0.14^{ab}	8.09 ± 0.01^a	8.07 ± 0.15^a	8.17 ± 0.02^a	8.05 ± 0.18^a
Radish	0 ($\mu\text{g mL}^{-1}$)	25 ($\mu\text{g mL}^{-1}$)	50 ($\mu\text{g mL}^{-1}$)	75 ($\mu\text{g mL}^{-1}$)	100 ($\mu\text{g mL}^{-1}$)	200 ($\mu\text{g mL}^{-1}$)
DPPH (mmol TE g^{-1} DW)	2.74 ± 0.11^b	2.75 ± 0.23^b	3.16 ± 0.19^a	3.35 ± 0.04^a	3.34 ± 0.12^a	3.27 ± 0.26^a
ABTS (mmol TE g^{-1} DW)	6.98 ± 0.33^b	7.07 ± 0.22^b	7.15 ± 0.32^b	7.69 ± 0.24^a	7.67 ± 0.22^a	7.67 ± 0.25^a

^a Different lower-case letters indicate significant differences among groups ($P < 0.05$).

$\mu\text{g mL}^{-1}$, with no further significant changes at higher concentrations.

These findings indicated that 5h-ChNF treatment significantly enhanced the antioxidant capacity of both broccoli and radish microgreens compared to their respective control groups. However, no significant differences were observed among most of the treated groups at higher concentrations. Microgreens are rich in a diverse group of antioxidants, making it challenging to determine which compounds contribute most to the observed effects.⁵³ However, considering polyphenols and flavonoids as the dominant contributors to the antioxidant activity in this study, it is not surprising that no further significant differences were observed at higher treatment concentrations.

4 Conclusions

Different ChNFs were successfully prepared from lobster shells *via* the DES method and APS oxidation. The yield and purity of DES-Chitin were up to $26.22 \pm 2.14\%$ and $94.78 \pm 0.39\%$, while the thermal stability remained unchanged when oxidized into ChNFs. APS oxidation effectively increased ChNFs crystallinity, carboxyl content, and dispersion stability, particularly in neutral or alkaline conditions. The morphological analysis revealed a progressive reduction in nanofiber size with extended oxidation time, contributing to improved transparency and dispersibility. The biological evaluation highlighted the potential of 5h-ChNF as a seed nanoprimer agent to enhance the growth, nutrient profiles, and antioxidant capacity of broccoli and radish microgreens. Optimal concentrations improved germination rates, root length, biomass accumulation, and leaf area while significantly boosting nitrogen assimilation, chlorophyll synthesis, protein, polyphenol, and flavonoid contents. Antioxidant activity, measured *via* DPPH and ABTS assays, also significantly increased compared to controls. However, excessive concentrations exhibited inhibitory effects on nutrient accumulation in broccoli, underscoring the importance of dose optimization. These findings provided a foundation that ChNFs derived from DES-Chitin could be sustainable nanomaterials for improving microgreen yield and nutritional value. Further research is warranted to elucidate their long-term physiological impacts and broader agricultural applications.

Data availability

The data used to support the findings of this study are included in the article.

Author contributions

Honglin Zhu: writing – review & editing, writing – original draft, methodology, formal analysis, conceptualization. Sunni Chen: writing – review & editing, writing – original draft. Jingyi Xue: writing – review & editing. Ruiqi Wang: writing – review & editing. Xinhao Wang: writing – review & editing. Zhenlei Xiao: writing – review & editing, methodology, funding acquisition, conceptualization. Yangchao Luo: writing – review & editing, methodology, funding acquisition, conceptualization.

Conflicts of interest

The authors declare that they have no known competing financial interests or personal relationships that could have appeared to influence the work reported in this paper.

Acknowledgements

This work was supported by the USDA National Institute of Food and Agriculture Hatch Multistate funds, accession number 7007849.

References

- 1 H. Zhu, T. Yang, S. Chen, X. Wang, J. He and Y. Luo, *Adv. Compos. Hybrid Mater.*, 2023, **6**, 192.
- 2 M. T. Zin, T. Kaewkod, J. Pekkoh, W. Pathom-aree, S. Chaipoot, G. Kanthakat, P. Seesuriyachan, Y.-Y. Chen, K. S. Khoo and B. Cheirsilp, *J. Agric. Food Res.*, 2025, 101673.
- 3 Y. Wang, H. Zhu, M. Qiao and Y. Luo, *Int. J. Biol. Macromol.*, 2024, **257**, 128714.
- 4 J. Lv, X. Lv, M. Ma, D.-H. Oh, Z. Jiang and X. Fu, *Carbohydr. Polym.*, 2023, **299**, 120142.
- 5 Y. Fan, T. Saito and A. Isogai, *Biomacromolecules*, 2008, **9**, 1919–1923.
- 6 S. Ifuku, M. Nogi, M. Yoshioka, M. Morimoto, H. Yano and H. Saimoto, *Carbohydr. Polym.*, 2010, **81**, 134–139.



- 7 Q. Wu, E. Jungstedt, M. Šoltéssová, N. E. Mushi and L. A. Berglund, *Nanoscale*, 2019, **11**, 11001–11011.
- 8 D. Liu, S. Huang, H. Wu and J. Zhang, *Cellulose*, 2022, **29**, 8539–8549.
- 9 J. L. Shamshina and N. Abidi, *ACS Sustain. Chem. Eng.*, 2022, **10**, 11846–11855.
- 10 S. Huang, T. Liu, Y. Liu, Y. Duan and J. Zhang, *Carbohydr. Polym.*, 2024, **340**, 122308.
- 11 N. Kandhol, V. P. Singh, N. Ramawat, R. Prasad, D. K. Chauhan, S. Sharma, R. Grillo, S. Sahi, J. Peralta-Videa and D. K. Tripathi, *Plant Stress*, 2022, **5**, 100091.
- 12 H. Imtiaz, M. Shiraz, A. R. Mir, H. Siddiqui and S. Hayat, *J. Plant Growth Regul.*, 2023, **42**, 6870–6890.
- 13 H. Zhu, S. Chen, J. Xue, X. Wang, T. Yang, J. He and Y. Luo, *Int. J. Biol. Macromol.*, 2025, 139762.
- 14 A. Rónavári, H. Kovács, Á. Szepesi, P. Pálfi, D. Ménesi and Z. Kónya, *29th International Symposium on Analytical and Environmental Problems*, 2023, pp. 195–199.
- 15 S. Selim, N. Akhtar, E. El Azab, M. Warrad, H. H. Alhassan, M. Abdel-Mawgoud, S. K. Al Jaouni and H. Abdelgawad, *Plants*, 2022, **11**, 306.
- 16 A. do Espirito Santo Pereira, H. Caixeta Oliveira, L. Fernandes Fraceto and C. Santaella, *Nanomaterials*, 2021, **11**, 267.
- 17 J. L. Shamshina, A. Kelly, T. Oldham and R. D. Rogers, *Environ. Chem. Lett.*, 2020, **18**, 53–60.
- 18 H. Zhu, S. Chen, T. Yang, X. Hu, W. Cai, X. Wang, J. He and Y. Luo, *Int. J. Biol. Macromol.*, 2024, **277**, 134425.
- 19 Q. Ma, K. Pang, K. Wang, S. Huang, B. Ding, Y. Duan and J. Zhang, *Carbohydr. Polym.*, 2019, **211**, 118–123.
- 20 S. Tanpichai, L. Pumpuang, Y. Srimarut, W. Woraprayote and Y. Malila, *Sci. Rep.*, 2023, **13**, 13195.
- 21 H. Zhu, S. Chen, H. Duan, J. He and Y. Luo, *Int. J. Biol. Macromol.*, 2023, **231**, 123213.
- 22 J. Xue, Y. Luo, B. Balasubramanian, A. Upadhyay, Z. Li and Y. Luo, *Food Hydrocolloids*, 2021, **120**, 106987.
- 23 M. R. Fayeziadeh, N. A. Ansari, M. M. Sourestani and M. Hasanuzzaman, *Plants*, 2023, **12**, 2652.
- 24 M. D. Ghoora, A. C. Haldipur and N. Srividya, *J. Agric. Food Res.*, 2020, **2**, 100046.
- 25 H.-l. Zhu, G. Chen, S.-n. Chen, Q.-r. Wang, L. Wan and S.-p. Jian, *Eur. Food Res. Technol.*, 2019, **245**, 1487–1498.
- 26 M. Muzolf-Panek and K. Stuper-Szablewska, *J. Food Meas. Charact.*, 2021, **15**, 4561–4574.
- 27 W. Cai, H. Zhu, Y. Luo and Q. Huang, *Int. J. Biol. Macromol.*, 2024, **281**, 136543.
- 28 A. C. Leung, S. Hrapovic, E. Lam, Y. Liu, K. B. Male, K. A. Mahmoud and J. H. Luong, *Small*, 2011, **7**, 302–305.
- 29 E. Mascheroni, R. Rampazzo, M. A. Ortenzi, G. Piva, S. Bonetti and L. Piergiovanni, *Cellulose*, 2016, **23**, 779–793.
- 30 A. A. Oun and J.-W. Rhim, *Carbohydr. Polym.*, 2017, **175**, 712–720.
- 31 K. Zhang, P. Sun, H. Liu, S. Shang, J. Song and D. Wang, *Carbohydr. Polym.*, 2016, **138**, 237–243.
- 32 Q. Wang, X. Yan, Y. Chang, L. Ren and J. Zhou, *Carbohydr. Polym.*, 2018, **180**, 81–87.
- 33 H. Zhu, S. Parvinian, C. Preston, O. Vaaland, Z. Ruan and L. Hu, *Nanoscale*, 2013, **5**, 3787–3792.
- 34 R. H. Müller and C. Jacobs, *Int. J. Pharm.*, 2002, **237**, 151–161.
- 35 Y. Fan, T. Saito and A. Isogai, *Biomacromolecules*, 2008, **9**, 192–198.
- 36 A. T. Paulino, J. I. Simionato, J. C. Garcia and J. Nozaki, *Carbohydr. Polym.*, 2006, **64**, 98–103.
- 37 Y. Yuan, S. Hong, H. Lian, K. Zhang and H. Liimatainen, *Carbohydr. Polym.*, 2020, **236**, 116095.
- 38 H. Zhu, S. Chen, J. Xue, X. Wang, Z. Xiao and Y. Luo, *J. Agric. Food Res.*, 2025, 101680.
- 39 Y.-j. Guan, J. Hu, X.-j. Wang and C.-x. Shao, *J. Zhejiang Univ., Sci., B*, 2009, **10**, 427–433.
- 40 N. Kananont, R. Pichyangkura, S. Chanprame, S. Chadchawan and P. Limpanavech, *Sci. Hortic.*, 2010, **124**, 239–247.
- 41 V. Saharan, R. Kumaraswamy, R. C. Choudhary, S. Kumari, A. Pal, R. Raliya and P. Biswas, *J. Agric. Food Chem.*, 2016, **64**, 6148–6155.
- 42 R. Li, J. He, H. Xie, W. Wang, S. K. Bose, Y. Sun, J. Hu and H. Yin, *Int. J. Biol. Macromol.*, 2019, **126**, 91–100.
- 43 Y. Cheng, Y. Wang, Y. Han, D. Li, Z. Zhang, X. Zhu, J. Tan and H. Wang, *Molecules*, 2019, **24**, 1752.
- 44 T. Zhan, C. Hu, Q. Kong, G. Shi, Y. Tang, Y. Zhou, Z. Guo, H. Zhai, X. Xiao and X. Zhao, *Sci. Total Environ.*, 2021, **799**, 149414.
- 45 A. Hassan, S. Gulzar and I. A. Nawchoo, in *Advances in Plant Nitrogen Metabolism*, CRC Press, 2022, pp. 86–95.
- 46 C. Wu, Z. Wang, H. Sun and S. Guo, *Frontiers of Forestry in China*, 2006, **1**, 170–175.
- 47 S. Pareek, N. A. Sagar, S. Sharma, V. Kumar, T. Agarwal, G. A. González-Aguilar and E. M. Yahia, *Fruit and Vegetable Phytochemicals: Chemistry and Human Health*, 2nd edn, 2017, pp. 269–284.
- 48 A. Fathi, *Agrisost*, 2022, **28**, 1–8.
- 49 M. A. U. Asad, X. Guan, L. Zhou, Z. Qian, Z. Yan and F. Cheng, *Plant Sci.*, 2023, **336**, 111855.
- 50 X. Liu, B. Hu and C. Chu, *J. Genet. Genomics*, 2022, **49**, 394–404.
- 51 J. Ková ik, M. Rep ák and I. Korn, *Acta Physiol. Plant.*, 2006, **28**, 159–164.
- 52 Z. Xiao, G. E. Lester, Y. Luo and Q. Wang, *J. Agric. Food Chem.*, 2012, **60**, 7644–7651.
- 53 L. Tan, H. Nuffer, J. Feng, S. H. Kwan, H. Chen, X. Tong and L. Kong, *Food Sci. Hum. Wellness*, 2020, **9**, 45–51.

